Tunable continuous-wave THz generator based on difference frequency generation with DAST crystal*

WANG Zelong[1, 2], WANG Yuye[1, 2, *], LI Haibin[1, 2], ZHANG Jingxi[1, 2], XU Degang[1, 2], YAO Jianquan[1, 2]

1. School of Precision Instrument and Optoelectronics Engineering, Tianjin University, Tianjin 300072, China

2. Key Laboratory of Optoelectronic Information Technology (Ministry of Education), Tianjin University, Tianjin 300072, China

Abstract

The terahertz (THz) difference frequency generation (DFG) based on DAST crystal has the advantages of wide tuning and room temperature operation. However, the low melting point and thermal conductivity of DAST crystal result in severe thermal accumulation and easy crystal damage under continuous pumping conditions, which limits its practical application. This article theoretically studies the thermal distribution characteristics of DAST crystals with diamond substrates, and experimentally analyzes the improvement of thermal effects of the substrates of DAST crystals. Furthermore, a THz-DFGTHz was constructed based on a diamond substrate DAST crystal pumped by continuous single frequency lasers. The frequency tuning range THzwas 1.1-3 THz, and the maximum output power of 3.39 nW was obtained at 2.493 THz. The power instability of the THz wave within 30 minutes was 2.19% This narrow linewidth, tunable THz source has high potential for applications in high-precision spectral detection and other fields

* The paper is an English translated version of the original Chinese paper published in *Acta Physica Sinica*. Please cite the paper as: WANG Zelong, WANG Yuye, LI Haibin, ZHANG Jingxi, XU Degang, YAO Jianquan, Tunable continuous-wave terahertz generator based on difference frequency generation with DAST crystal. *Acta Phys. Sin.* 2025, 74(3): 034201. doi: 10.7498/aps.74.20241349

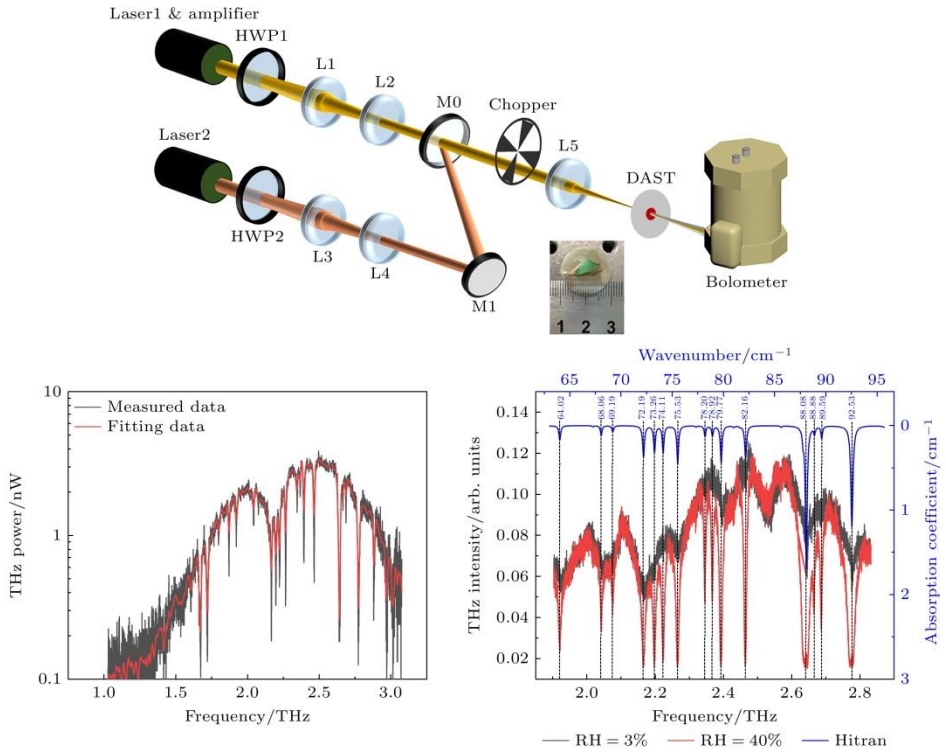

Keywords: continuous-wave THz source, difference frequency generation , DAST crystal

PACS: 42.55.Rz; 42.60.-v; 42.62.Fi; 42.65.-k

doi: 10.7498/aps.74.20241349
cstr: 32037.14.aps.74.20241349

1. Introduction

THz band is located between infrared and microwave in the electromagnetic spectrum, which has important application prospects in astronomy, atmospheric science, basic physics, wireless communication, biomedical and other fields.[1-6]. In recent years, spectral detection techniques, such as THz time-domain spectroscopy, have achieved specific fingerprint identification characterization by directly measuring the inherent vibrational/rotational information of the molecular of the samples[7]. With the further development of THz field, the research and exploration of broadband tunable, narrow linewidth and high stability THz source has become a hotspot.

At present, there are several methods to generate narrow linewidth THz wave, such as solid-state semiconductor electronics technology[8], free-electron laser[9], quantum cascade laser[10], CO_2 pumped gas laser[11], THz time-domain spectroscopy technology and nonlinear optical frequency conversion technology[12,13]. Schottky diode solid state

frequency multiplier and resonant tunneling diode oscillator based on solid state semiconductor electronics can generate high stability and narrow linewidth THz wave, but due to the performance of the core device diode, it is difficult to achieve high frequency THz wave output above 1 THz, so that the tuning range is limited. THz generation by free electron laser has excellent properties such as narrow linewidth, high power, broadband tunability, but the high manufacturing and usage costs make it difficult to be widely applied for research. Quantum cascade laser is an effective way to generate high frequency and narrow linewidth THz wave, but its narrow output bandwidth and tuning gap limit its further application in the field of spectral detection. CO_2 pumped gas laser can output single-frequency high-power THz wave, but the frequency tuning is realized by replacing pump gas, which is not suitable for the field of spectral detection. THz time-domain spectroscopy based on ultrashort pulse pumping is one of the most mature commercial THz radiation sources, but its GHz level linewidth and low signal-to-noise ratio in high frequency band make it difficult to meet the needs of high-precision spectral detection of gas molecules. In the field of THz wave generation technology based on nonlinear optical frequency conversion, it is mainly divided into THz parametric radiation source and THz difference frequency radiation source[14 - 16]. In the process of THz wave generation, the linewidth of THz wave is directly related to the linewidth of the pump laser, so compared with the pulsed laser pump ,of which linewidth is limited by the Fourier limit, using continuous laser as the pump light has more advantages in generating narrow-linewidth THz waves[17]. THz parametric generator/oscillator is difficult to achieve widely tunable THz wave output because of its high threshold and low power density of continuous pump[18]. For DFG, the continuous wave THz difference frequency source based on VECSEL can output 100 μW THz wave with a linewidth of 100 kHz, but due to the characteristics of the pump laser and the crystal, it can only output THz wave at 1.9 THz, which is difficult to be further applied to broadband spectral detection and other fields[19]. Nonlinear crystal is one of the key factors to determine the performance of THz-DFG. At present, the nonlinear crystals mainly include inorganic crystals and organic crystals. Inorganic crystals mainly include $LiNbO_3$, GaAs, $ZnGeP_2$, GaP, ZnTe, etc. These crystals have a large refractive index difference between infrared and THz bands (such as $LiNbO_3$ crystal, of which refractive index is 2.1 and 5.2 in infrared and THz bands, respectively), the absorption of THz wave by the crystal increases with the increase of frequency, so that the range of output THz wave is narrow[20]. For organic crystals, although the melting point and thermal conductivity are lower than those of inorganic crystals, but the high effective nonlinear coefficients (the d_{eff} of DAST are 1010 pm/V), which have obvious advantages over inorganic crystals (the d_{eff} of $LiNbO_3$ is 27 pm/V, and the

d_{eff} of $ZnGeP_2$ is 75 pm/V).In addition, the refractive index curve of the organic crystal is relatively flat, so that the organic crystal meets the type 0 phase matching condition that the infrared and THz waves are collinear and have the same polarization direction, the tunable output of the THz wave can be realized only by changing the pump wavelength [21]. However, due to the low melting point and low thermal conductivity of organic crystals, the internal heat accumulation of crystals is easily lead to thermal damage of crystals under high repetition rate or continuous pumping conditions, which limits their further applications[22].

In this paper, the thermal distribution of DAST crystal with diamond substrate under continuous pumping was theoretically studied. It was experimentally verified that the diamond substrate can effectively improve the thermal damage threshold. Furthermore, a THz-DFG based on continuous fiber lasers pump and DAST crystal with diamond substrate was constructed. The continuous THz wave with tunable frequency from 1.1 THz to 3 THz was realized, the maximum power was 3.39 nW at 2.493 THz. The power fluctuation was measured to be 2.19% in 30 min. Moreover, the high-precision spectral detection of air with different humidity was measured by this THz-DFG, the results were in good correspondence with the gas absorption lines in the Hitran database.

2. Simulation and Experimental Analysis of Thermal Effect of DAST Crystal

Under nanosecond (ns) pulsed pumping, the damage thresholds of organic crystals were on the order of GW/cm ². However, under continuous-wave (CW) pumping, the damage mechanism was fundamentally changed, the thresholds tested by pulse pump were no longer applicable. Due to the low thermal conductivity and low melting point of organic crystals, the internal heat accumulation was easily lead to thermal damage of the crystal under high power pumping, which would reduce the output power and the stability of THz-DFG. Integrating a heat dissipation substrate can enhance the thermal damage threshold of the crystals by improving heat extraction. The thickness of DAST crystal commonly used in DFG was hundreds of microns, and it was difficult by using copper, aluminum, indium and other metal materials to dissipate heat from the side of the crystal. Thus, using the substrate material to attach to the crystal surface would be a good way to increase the contact area between the crystal and the substrate. In the selection of heat dissipation materials, it was necessary to meet the conditions of high thermal conductivity, high transmittance, can be optical polishing of surface and stable chemical properties, commonly used materials were diamond, sapphire and silicon. The absorption coefficients of these three materials

were below 0.1 cm^{-1} in the pump range, so the transmittance of the pump light was mainly affected by the refractive index of materials ($n_{Diamond}$ = 2.2, $n_{sapphire}$ = 1.8, n_{Si} = 3.4). Considering that the thermal conductivity of silicon was 148 W/(m • K), that of sapphire was only 25 W/(m •K), and that of diamond was 1800 W/(m •K). Therefore, the diamond-DAST structure was expected to improve the heat dissipation effect of DAST crystal.

Firstly, the the thermal distribution of DAST crystal was stimulated based on COMSOL Multiphysics. The mainly parameters were as follows: the radius of DAST crystal was 3 mm, the thickness was 0.5 mm, the melting point of DAST crystal was 256 ℃, the thermal conductivity was 0.255 W/(m • K), and the heat capacity at constant pressure was 1.156 J/(G • K). The incident wavelength was 1536.8489 nm, the waist radius was 50 μ m, and the intensity distribution was Gaussian beam. The thermal conductivity of the diamond substrate was 1800 W/(m • K), and the transmittance in the near infrared band was 65%. The ambient temperature was maintained at 18 ℃. Fig. 1(a) illustrates the thermal distribution of DAST crystal without substrate. Under a total pump power of 3 W, the central region of DAST crystal reaches a peak temperature of 404 ° C, while the edge temperature rose to approximately 40 ℃. This configuration generates a substantial internal temperature gradient (Δ T≈364 ℃), inducing strong thermal stress within the crystal. Once the local temperature exceeds the melting point, the crystal will be rapidly melted and cause severe thermal damage. In contrast, Fig. 1(b) shows the simulation result of the heat distribution of the case which the crystal with the diamond substrate. It can be seen that the maximum temperature of DAST crystal was reduced to 216 ℃ (edge: 25 ℃), and the temperature gradient in the crystal was also reduced, thus effectively reducing the thermal stress in the crystal and enhancing the resistance of the crystal to thermal damage.

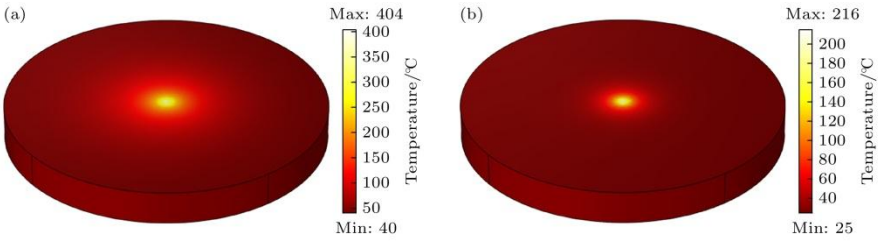

Figure 1. Simulation results of heat distribution of organic crystals: (a) Without and (b) with diamond substrate.

The thermal distribution in the DAST crystal at different pump powers was theoretically simulated, of which the results were shown in Fig. 2. Fig. 2(a) shows that the temperature of both DAST crystal and Diamond-DAST crystal increases rapidly

with the increase of pump power. When the pump power was up to 4.5 W, the maximum temperature in the center of the DAST crystal without substrate reached 584 ℃. While the temperature trend of the crystal with diamond substrate was obviously flattened, the maximum temperature only rose to 304 ℃. It can be seen that the diamond substrate had significant effect on controlling the temperature in the center of the DAST crystal. Fig. 2(b) shows the relationship between the lowest temperature at the crystal edge and the pump power. With the increase of the pump power to 4.5 W, the lowest temperature at the edge of the DAST crystal increases to 48 ℃, while it was only 27 ℃ in Diamond-DAST crystal. The diamond substrate had good heat dissipation effect which can effectively reduce the temperature of the crystal and the internal temperature difference. Therefore, by reducing the temperature and the thermal stress in the crystal, the diamond substrate can effectively increase the upper limit of the pump power.

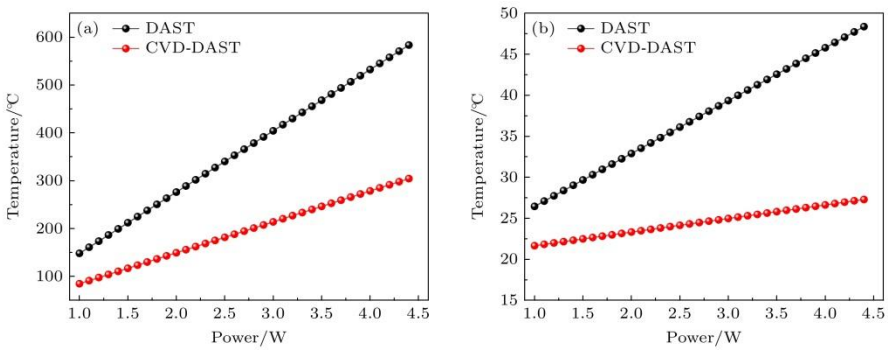

Figure 2. Curves of crystal temperature variation with pump power: (a) Maximum temperature; (b) minimum temperature.

Fig. 3(a) illustrates the schematic diagram of the Diamond-DAST crystal used in the experiment. The DAST crystal was closely attached to the diamond substrate, the thickness of the DAST crystal was 0.8 mm. The diameter and the thickness of the diamond substrate were 30mm and 0.4 mm, respectively. The radius of the pump laser waist was 50 μm, the wavelength was 1536.8489 nm and the maximum power was 3 W. For the DAST crystal without diamond substrate, when the pump power exceeds the thermal damage threshold of the DAST crystal, the crystal will gradually melt from the center of the focus spot at the surface to the interior of crystal, the circular melting damage was shown in Fig. 3(b). Fig. 3(c) shows the surface of Diamond-DAST crystal. It can be seen that there was no thermal damage on the inner surface of Diamond-DAST under the same pumping conditions. Using a microscope to illuminate the same position of the crystal, the slight internal thermal damage of the crystal can be observed as shown in Fig. 3(d), but the phenomenon of crystal melting

did not occur. When the pump power or pump time was further increased, the Diamond-DAST crystal will gradually melt from the interior to the Surface B. The results of surface melting through Surface B are shown in Fig. 3(e), it can be seen that the damage area was irregular. The experimental results showed that the diamond substrate can effectively improve the thermal effect in the DAST crystal, but due to low thermal conductivity of the organic crystal, the heat generated in the interior of the crystal can not be effectively conducted to the diamond surface, so that the thermal damage still exists. It can be concluded that thinner crystal could have better heat dissipation effect.

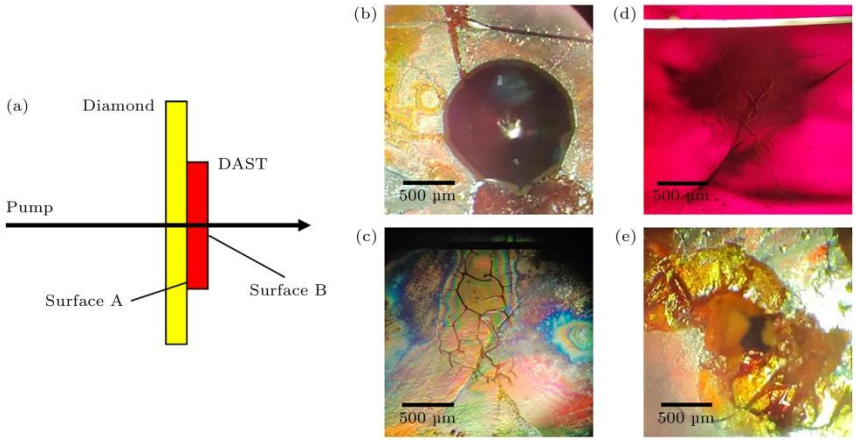

Figure 3. (a) Schematic diagram of thermal damage experiment; (b) Thermal damage surface of DAST crystal (c) Surface of Diamond-DAST crystal; (d) Inside the diamond-DAST crystal, (e) Outer surface of the Diamond-DAST crystal.

Due to high roughness of the organic crystal surface, the exit spot of the laser transmitted through the crystal will produce a certain distortion. In the experiment, the interior structure change of the crystal can be obtained by observing the shape change of the residual pump light. The results of crystal thermal damage at different powers were listed in Tab.1. It can be seen from Tab.1 that when the pump power reached 0.75 W, the crystal without diamond substrate was deformed due to thermal stress, resulting in irreversible thermal damage. When the pump power reached 1.20 W, the melting phenomenon occurred at the incident surface. For Diamond-DAST crystal, the unrecoverable damage caused by thermal stress appears when the pump power was increased to 1.70 W, and it gradually melts from the interior of the crystal to Surface B when the pump power is increased to 2.65 W. Therefore, the diamond substrate can absorb the heat generated in the organic crystal. When continuous laser pumped, it could effectively reducing the temperature of the organic crystal, and increasing the upper limit of the pump power that the THz-DFG with Diamond-DAST crystal could generate higher THz wave output.

Table 1. Dependence of pump power and thermal damage of DAST crystal with/without diamond substrate.

	Crystal transformation	Thermal stress causes tiny deformation of recoverable in the crystal (recoverable by reducing the power)	The thermal stress causes the unrecoverable deformation of in the crystal (unrecoverable by reducing the power)	Crystal melting
DAST	$P < 0.45$ W	0.45 W $\leq P < 0.75$ W	0.75 W $\leq P < 1.20$ W	$P \geq 1.20$ W
Diamond-DAST	$P < 1.10$ W	1.10 W $\leq P < 1.70$ W	1.70 W $\leq P < 2.65$ W	$P \geq 2.65$ W

3. Experimental Results and Analysis of Narrow Linewidth Difference Frequency Source

The schematic diagram of the continuous THz-DFG was shown in Fig. 4. Laser1 (T100S-HP, EXFO Inc.) can generate a ~mW narrow linewidth polarized light in the range of 1500-1630nm, which was then boosted to the maximum power of 15W in the range of 1545-1561nm (λ_1) by an amplifier (KEOPSYSCEFA-C-PB-HP,LumibirdInc.), the fluctuation was 1.27% in 30 minutes. Laser2 (CoSF-D-ER-B-MP, Connet Fiber Optics Co. Ltd.) can generate narrow linewidth CW light at a fixed wavelength of 1536.8489nm (λ_2), of which the maximum power and the fluctuation in 30 minutes were 10W and 0.62%, respectively. Half-wave plates (HWP1, HWP2) were used to adjust the polarization direction of the dual-wavelength pump light. L1 and L2, L3 and L4 formed a convergent beam collimation system, which adjusted the beam waist radius and divergence angles of λ_1 and λ_2 to be close to each other. Then, M0 and M1 were used to combines these tow beams into one line. In order to improve the pump power density in DFG process, the combined dual-wavelength pump light was focused by L5 and incident to the Diamond-DAST crystal. The thickness of the Diamond-DAST crystal in the experiment was 0.54 mm. The photograph of the crystal was shown in the inset of Fig. 4. The *a* axis of the crystal was parallel to the polarization of the dual-wavelength beam to meet the phase matching condition. A liquid helium-cooled Bolometer was used for power detection with a response sensitivity of 2.89×10^5 V/W, The black polyethylene (PE) sheet was inserted before the detection window of 4K-Bolometer to filter out the residual NIR signal and stray light. Considering the response rate of Bolometer, a chopper with a frequency of 100 Hz was used in the optical path.

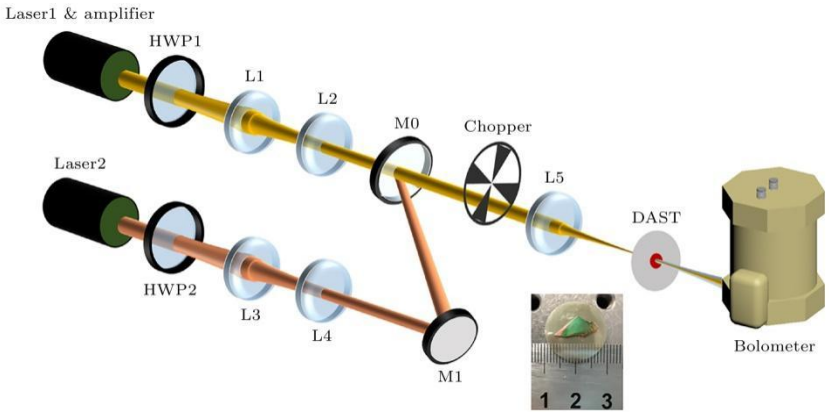

Figure 4. Schematic diagram of the CW-THz source. The inset is DAST crystal with diamond substrate.

After adjusting the polarization directions of two pump light to be the same, the polarization characteristics of dual-wavelength were measured by a Glan prism, the results were shown in Fig. 5(a). It can be seen that the dual-wavelength pump had good linear polarization characteristics, the polarization extinction ratio was 17.96 dB. Besides, the wavelength stability of the dual-wavelength beam at different wavelengths was measured by a wavelength meter (AQ6151, Yokogawa Co. Ltd.), the results were shown in the Fig. 5(b). It can be seen that the wavelength drift was less than ±2 pm within 30 min. The inset shows the wavelength tuning curve where the dual-wavelength pump power was 1:1, the total output power was set to 4 W, and the power variation of λ_2 was within ±0.22 W during the tuning process from 1545 nm to 1561 nm.

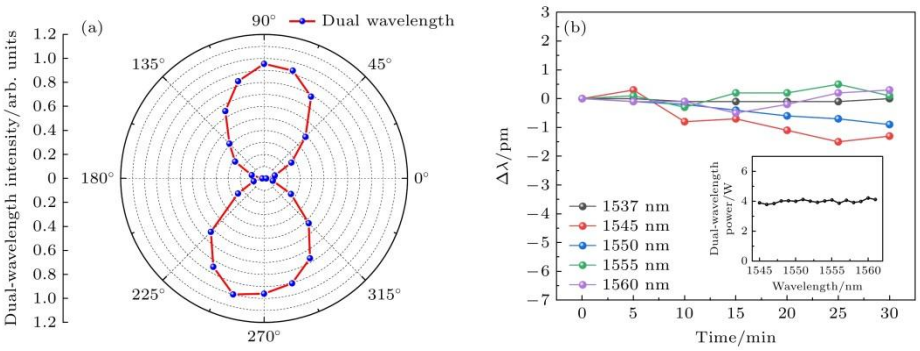

Figure 5. (a) Polarization characteristics of the dual-wavelength pump, (b) Wavelength stability and the inset is power tuning characteristics

In the experiment, the power of the dual-wavelength pump was set to 4 W, where the power ratio was 1:1. When the wavelength scanning range of the λ_2 was 1545-1561 nm, the corresponding frequency of the THz output range was 1.1-3 THz. The output characteristics were shown in Fig. 6(a). The red solid line in the figure was the fitting curve after denoising the measured output spectra. It can be seen that there were many

output valleys in the narrow linewidth output spectra which were mainly caused by the strong absorption of water vapor in the air. The THz output power reaches the maximum of 3.39 nW at 2.493THz, the conversion efficiency was 0.85×10^{-9}, which was 22% higher than that of the non-heat dissipation crystal[23]. Due to the strong absorption caused by the resonance of the transverse optical phonon around 1.1 THz, the THz power in the range of 1.1-1.4 THz was relatively low, and there was a ~nW level THz wave output in the range of 1.4-3.0 THz. Fig. 6(b) shows the power stability curve at the output frequency of 2.493 THz. It can been seen that the decay of the THz output had not been observed in 30 min of laser illumination at the power of 4 W, the fluctuation of THz power was 2.19%. The polarization of the THz wave was measured using a THz wire grid, and the results were shown in the inset of Fig. 6(b). The polarization extinction ratio of the THz wave was 9.44 dB. Based on the measurement results, it can be seen that the THz-DFG has high power stability and good linear polarization.

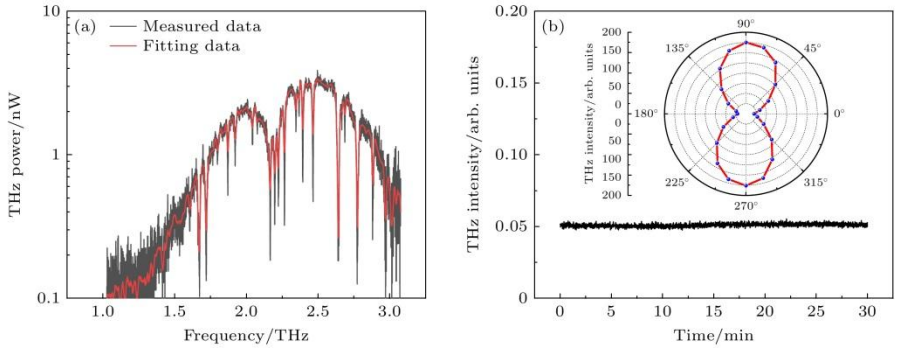

Figure 6. (a) Tunable characteristics of the CW-THz source. (b) Stability of the generated THz power over a time frame of 30 min, and the inset is polarization characteristics of the THz wave @ 2.493 THz

Fig. 7(a) shows the output characteristic curve of the THz-DFG at 1.697, 2.056 and 2.493 THz, the pump power ratio was 1:1. From the figure, it can be seen that the output intensity of THz wave increases with the increase of pump power at different frequencies, and there was no obvious saturation trend. The dependence between the THz wave intensity and the change of the power of λ_1 or λ_2 at 2.493 THz were shown in Fig. 7(b), where the red and black curve were the influence of the power of λ_1 and λ_2 to the output intensity of THz wave, respectively. Due to the low pump power density, the intensity of THz wave was slightly sensitive to the power change of short wavelength (λ_1). When the pump power was further increased, the influence of the power of λ_1 on the intensity of THz wave would be more significant than that of λ_2.

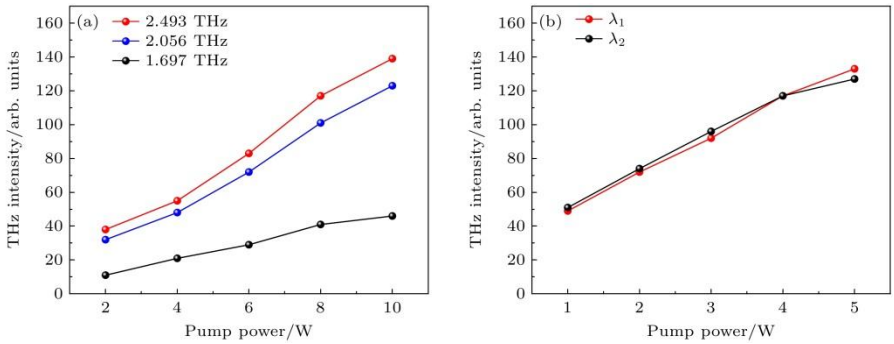

Figure 7. The dependence of the THz wave intensity and (a) the dual-wavelength pump power, (b) the pump power of λ_1 or λ_2.

In order to verify the application potential of this THz-DFG in high-precision spectral detection, the transmission spectra of air at different humidity were detected in the frequency range of 1.90-2.85 THz. The optical path was 15 cm, the humidity of air were set to be 40% and 3%. The red line in Fig. 8 was the transmission spectrum of 40% humidity air. The blue line was also showed the absorption lines of water vapor in THz band in the Hitran database[24]. It can be seen from Fig. 8 that there were 15 obvious absorption peaks of water vapor in the spectra range, the position of all these peaks were well correspond to the position of transmission dips accurately. For the absorption peak with small absorption coefficient, the dip value of the transmission spectra was in good agreement with the intensity of the water vapor absorption peak. For the absorption peak with large absorption coefficient, the transmission dip was close to the background noise due to the long experimental optical path. In order to compare the absorption difference of THz wave by water vapor in the air under different humidity conditions, the humidity was reduced to a minimum of 3% by continuously introducing dry air and keeping other experimental conditions still. Under this condition, the transmission spectrum was shown by black line in Fig. 8. Compared with the results of 40% humidity, most of the transmission dips caused by water vapor basically disappear, thus, the humidity in the air had a great impact on the THz spectrum. Even though the humidity was at a low level of 3%, the absorption of water vapor in THz band was very strong, the transmission dips at 88.08 cm^{-1} and 92.53 cm^{-1} were still obvious in the air transmission spectrum.

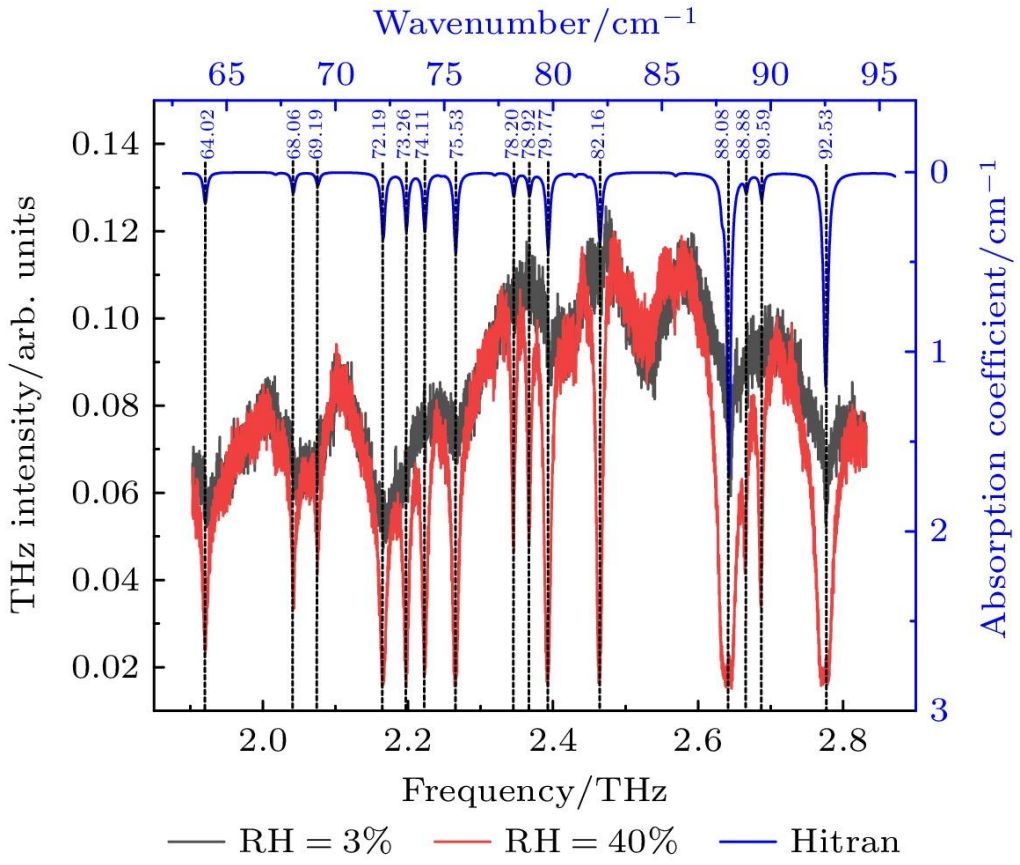

Figure 8. Transmission characteristics of air with different humidity of 1.90-2.85 THz

4. Conclusion

In this paper, the thermal distribution characteristics of continuous pumped DAST crystal with/without diamond substrate were simulated. Two single-frequency fiber lasers were used to pump the Diamond-DAST crystal to generate THz wave by DFG. The results show that the output frequency range of THz wave was 1.1-3 THz, the maximum output power was 3.39 nW at 2.493 THz. The power fluctuation was 2.19% in 30 min. In addition, the high precision transmission spectra of air with different humidity were measured by this THz-DFG, the results were in good agreement with the gas absorption lines in Hitran database. This continuous THz-DFG has the advantages of narrow linewidth, high accuracy tuning and high power stability, which makes it has high application potential in THz high-precision spectrum detection, imaging fields.

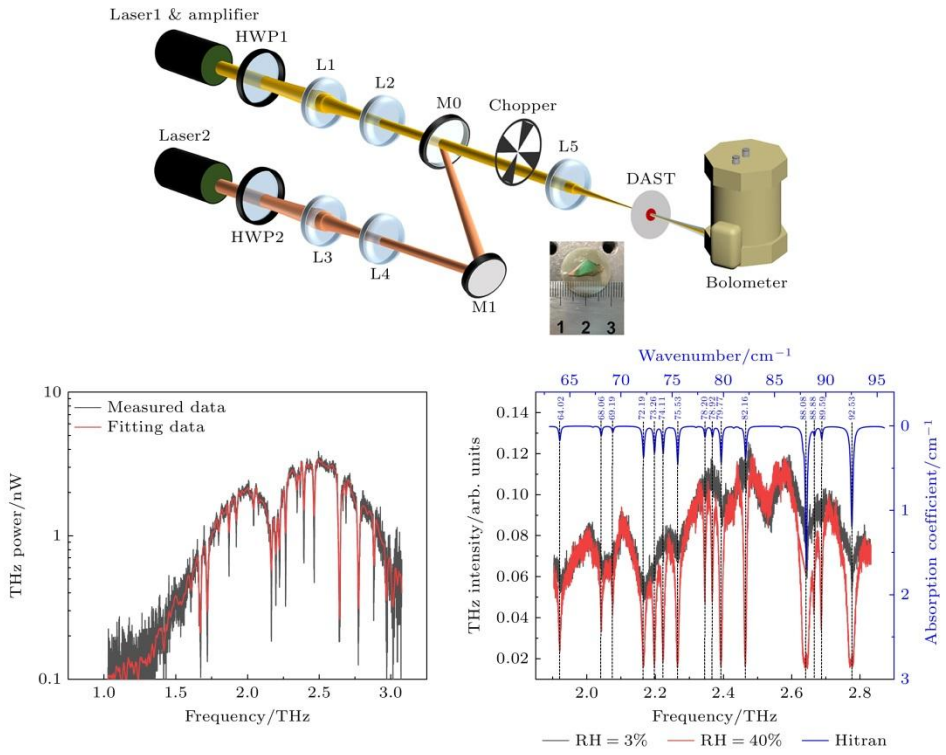

References

[1] Ferguson B, Zhang X C 2002 *Nat. Mater.* **1** 26

[2] Sirtori C 2002 *Nature* **417** 132

[3] Sterczewski L A, Westberg J, Yang Y, Burghoff D, Reno J, Hu Q, Wysocki G 2020 *ACS Photonics* **7** 1082

[4] Stinson H T, Sternbach A, Najera O, Jing R, McLeod A S, Slusar T V, Mueller A, Anderegg L, Kim H T, Rozenberg M, Basov D N 2018 *Nat. Commun.* **9** 3604

[5] Mu N, Yang C Y, Ma K, Quan Y L, Wang S, Lai Y, Li F, Wang Y Y, Chen T N, Xu D G, Feng H 2022 *Acta Phys. Sin.* **71** 178702

[6] Wang Y W, Dong Z W, Li H Y, Zhou X, Luo Z F 2016 *Acta Phys. Sin.* **65** 134101

[7] Yang X, Zhao X, Yang K, Liu Y, Liu Y, Fu W, Luo Y 2016 *Trends Biotechnol.* **34** 810

[8] Aghasi H, Naghavi S M H, Taba M T, Aseeri M A, Cathelin A, Afshari E 2020 *Appl. Phys. Rev.* **7** 021302

[9] Cherkassky V S, Knyazev B A, Kubarev V V, Kulipanov G N, Kruyshev G L, Matveenko A N, Petrov A K, Petrov V M, Scheglov M A, Shevchenko O A, Vmokurov N A 2004 *Joint 29th International Conference on Infrared and Millimeter Waves and 12th International Conference on Teraheriz Electronics* Karlsruhe, Germany, September 17–October 1, 2004 p567

[10] Chhantyal-Pun R, Valavanis A, Keeley J T, Rubino P, Kundu I, Han Y, Dean P, Li

L, Davies A G, Linfield E H 2018 *Opt. Lett.* **43** 2225

[11] Mueller E R, Henschke R, Robotham W E, Newman L A, Laughman L M, Hart R A, Kennedy J, Pickett H M 2007 *Appl. Optics* **46** 4907

[12] Chen K, Tang L, Xu D, Wang Y, Yan C, Nie G, Hu C, Wu B, Zhu J, Yao J 2021 *ACS Photonics* **8** 3141

[13] Mansourzadeh S, Vogel T, Shalaby M, Wulf F, Saraceno C J 2021 *Opt. Express* **29** 38946

[14] Lee A J, Pask H M 2014 *Opt. Lett.* **39** 442

[15] He Y, Wang Y, Xu D, Nie M, Yan C, Tang L, Shi J, Feng J, Yan D, Liu H, Teng B, Feng H, Yao J 2018 *Appl. Phys. B* **124** 16

[16] Chai L, Niu Y, Li Y F, Hu M L, Wang Q Y 2016 *Acta. Phys. Sin.* **65** 070702

[17] Tang M, Minamide H, Wang Y, Notake T, Ohno S, Ito H 2011 *Opt. Express* **19** 779

[18] Walsh D, Stothard D J M, Edwards T J, Browne P G, Rae C E, Dunn M H 2009 *J. Opt. Soc. Am. B: Opt. Phys.* **26** 1196

[19] Paul J R, Scheller M, Laurain A, Young A, Koch S W, Moloney J 2013 *Opt. Lett.* **38** 3654

[20] Liu H, Xu D G, Yao J Q 2008 *Acta. Phys. Sin.* **57** 5662

[21] Cunningham P D, Hayden L M 2010 *Opt. Express* **18** 23620

[22] Zhao H, Tan Y, Wu T, Steinfeld G, Zhang Y, Zhang C, Zhang L, Shalaby M 2019 *Appl. Phys. Lett.* **114** 241101

[23] Wang Z, Wang Y, Li H, Ge M, Xu D, Yao J 2023 *Opt. Express* **31** 39030

[24] Rothman L S, Jacquemart D, Barbe A, Benner D C, Birk M, Brown L R, Carleer M R, Chackerian C, Chance K, Coudert L H, Dana V, Devi V M, Flaud J M, Gamache R R, Goldman A, Hartmann J M, Jucks K W, Maki A G, Mandin J Y, Massie S T, Orphal J, Perrin A, Rinsland C P, Smith M A H, Tennyson J, Tolchenov R N, Toth R A, Vander Auwera J, Varanasi P, Wagner G 2005 *J. Quant. Spectrosc. Radiat. Transfer* **96** 139